

# Nanoscale

Accepted Manuscript



This is an *Accepted Manuscript*, which has been through the Royal Society of Chemistry peer review process and has been accepted for publication.

*Accepted Manuscripts* are published online shortly after acceptance, before technical editing, formatting and proof reading. Using this free service, authors can make their results available to the community, in citable form, before we publish the edited article. We will replace this *Accepted Manuscript* with the edited and formatted *Advance Article* as soon as it is available.

You can find more information about *Accepted Manuscripts* in the [Information for Authors](#).

Please note that technical editing may introduce minor changes to the text and/or graphics, which may alter content. The journal's standard [Terms & Conditions](#) and the [Ethical guidelines](#) still apply. In no event shall the Royal Society of Chemistry be held responsible for any errors or omissions in this *Accepted Manuscript* or any consequences arising from the use of any information it contains.



## Nanoscale

## COMMUNICATION

## Quantification of proteins using enhanced etching of Ag coated Au nanorods by Cu<sup>2+</sup>/bicinchoninic acid pair with improved sensitivity

Received 00th January 20xx,  
Accepted 00th January 20xx

DOI: 10.1039/x0xx00000x

Wenqi Liu,<sup>a,b</sup> Shuai Hou,<sup>a,b</sup> Jiao Yan,<sup>a,b</sup> Hui Zhang,<sup>a,b</sup> Yinglu Ji,<sup>a</sup> and Xiaochun Wu\*<sup>a</sup>

www.rsc.org/nanoscale

Plasmonic nanosensors demonstrate great potentials in ultrasensitive detection, especially with plasmon peak position as detection modality. Herein, a new sensitive yet simple total protein quantification method termed SPR-BCA assay is demonstrated by combining plasmonic nanosensors with protein oxidation by Cu<sup>2+</sup>. The easy tuning of localized surface plasmon resonance (LSPR) features of plasmonic nanostructures makes them ideal sensing platforms. We found that Cu<sup>2+</sup>/bicinchoninic acid (BCA) pair exhibits accelerated etching of Au@Ag nanorods and results in the LSPR peak shift. A linear relationship between Cu<sup>2+</sup> and LSPR shift is found in a double logarithmic coordinate. Such a relation is transferred to the concentration of proteins. Theoretical simulation exhibits that Au nanorods with large aspect ratios and small core sizes show high detection sensitivity. Via optimized sensor design, we achieved an increased sensitivity (the limit of detection is 3.4 ng/ml) and a wide working range (0.5 to 1000 µg/ml) compared with traditional BCA assay. The universality to various proteins further proves its potential in practical applications.

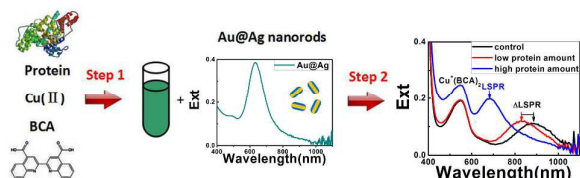
Nanosensors based on plasmonic structures have aroused intense scientific attention and exhibited outstanding performance in terms of sensitivity and operability (1, 2). Generally, three sensing modalities are employed including localized surface plasmon resonance (LSPR) peak shift or intensity changing from extinction spectra, surface-enhanced Raman scattering (SERS), and quenching or enhancement of molecule fluorescence by plasmonic nanoparticles (1). Among them, the assays based on the LSPR peak shift have demonstrated surprisingly high sensitivity in comparison with SERS and fluorescence methods apart from its high reproducibility and simple instrumentation. For instance, based on the peak shift of gold nanorods (Au NRs) caused by Cu<sup>2+</sup>-mediated formation of core-shell structure, detection of 2 femtomolar Cu<sup>2+</sup> is

achieved (3). As the LSPR peak position is closely related to the composition, refractive index of local microenvironment, and aggregation/agglomeration of nanoparticles, the three factors have been utilized for analyte detection (4-6). Among them, colorimetric nanosensors based on aggregation of spherical gold nanoparticles have been widely applied (7). Recently, based on the idea and in combination with traditional ELISA, Steven's group further developed a new kind of ELISA, called plasmonic ELISA (8). They demonstrated ultrasensitive detection of prostate specific antigen (PSA) and HIV-1 capsid antigen p24 utilizing significant color difference of gold nanoparticles in discrete or aggregated states. For the other two factors, generally, owing to similar refractive index of organic molecules and biomolecules, the peak shift caused by near distance dielectric sensitivity is often limited. In contrast, by forming inorganic shell, the induced LSPR peak shift can be quite large due to large shell dielectric constant and easy shell thickness tuning, thus providing more opportunities to realize high-sensitivity detection. With the help of such an idea, Steven's group used glucose oxidase to control the growth of Ag on gold nanorods, in turn to tailor the LSPR peak shift of the plasmonic sensors (9). They achieved ultrasensitive detection of PSA in whole serum.

Encouraged by the achievements based on plasmonic nanoparticle growth controlled by specific recognition of proteins, we wonder whether such a strategy can be extended to total protein quantification. Based on the high sensitivity of the LSPR peak on particle composition, we designed a sensing platform based on LSPR peak shift via controlled etching of Au@Ag nanorods. Combination of Au rod core with Ag shell provides an ideal SPR peak sensor (6, 10). The synthesis method of Au NRs is well-developed with easy tailoring in the LSPR peak position. Deposition of Ag shell could induce significant peak shift with additional benefit of peak narrowing owing to "plasmonic focusing" effect (11). We previously found that Cu<sup>2+</sup> can assist Ag dissolution from Au@Ag nanorods (12). By adding bicinchoninic acid (BCA), we observed direct etch of Ag by Cu<sup>2+</sup>/BCA pair via redox reaction  $\text{Cu}^{2+} + \text{Ag} + 2\text{BCA} \rightarrow \text{Cu}^+(\text{BCA})_2 + \text{Ag}^+$ . Strong binding of Cu<sup>+</sup> with BCA increases the oxidation capability of Cu<sup>2+</sup>. Connecting with oxidation of protein by Cu<sup>2+</sup> (13), we herein develop a new SPR-BCA assay to detect total protein with improved detection sensitivity. The

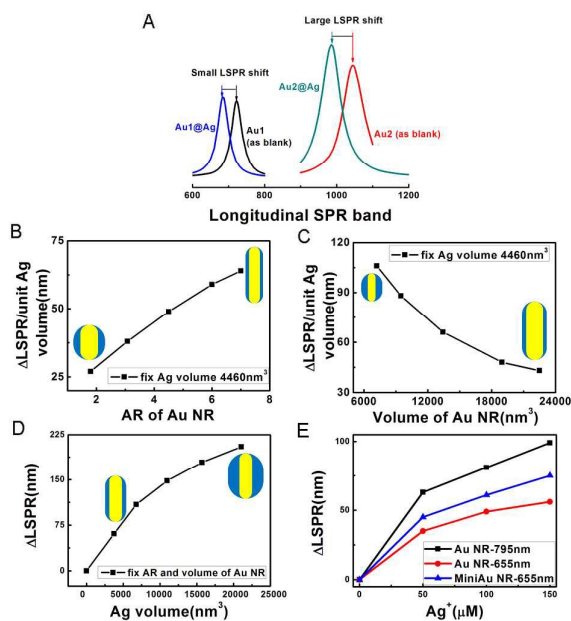
<sup>a</sup>CAS Key Laboratory of Standardization and Measurement for Nanotechnology, National Center for Nanoscience and Technology, Beijing 100190, P. R. China

<sup>b</sup>University of the Chinese Academy of Sciences, Beijing 100190, P. R. China  
Electronic Supplementary Information (ESI) available: [details of any supplementary information available should be included here]. See DOI: 10.1039/x0xx00000x



**New Scheme 1.** Quantification of proteins through Au@Ag nanorods etching by  $\text{Cu}^{2+}$ /BCA pair.

quantification principle includes two parts as shown in Scheme 1. The first part is protein oxidation by  $\text{Cu}^{2+}$  via incubating the mixture of protein,  $\text{Cu}^{2+}$ , and BCA at  $60^\circ\text{C}$  for a given time. During this process, parts of  $\text{Cu}^{2+}$  are reduced to  $\text{Cu}^+$  by protein and the obtained cuprous ions are chelated by BCA molecules. In the second step, the remaining cupric ions (after 60-fold dilution) are used to etch Au@Ag NRs with the help of BCA, resulting in the red-shift of the LSPR peak. The lower the protein amount is, the larger the LSPR is red-shifted. Based on the relationship between protein concentration and the LSPR shift, the protein amount is determined. As shown in Scheme 1 step 2, there is no  $\text{Cu}^{2+}$  consumption in the control sample which shows the maximal etching of the Ag shell. The control thus exhibits the largest red-shift of the LSPR. In our case, we tune the shifted LSPR of the control to that of close to Au core. In order to achieve a high sensitivity, we need to have a large peak difference between the control and the low protein sample. For rod-shaped noble metallic



**New Figure 1.** FEM simulation of response sensitivity based on LSPR peak shift: (A) Demonstration of improving sensitivity by increasing the aspect ratio of Au core. Effects of AR (B) and volume (C) of the Au NR core, as well as Ag shell volume (D) on Au@Ag sensitivity. (E) Experimental results of the LSPR peak shift after growing different volumes of Ag shell on three different Au NR cores.

nanoparticles, aspect ratio (AR) of the rod plays a key role in determining the LSPR peak position. The Au nanorods with a large AR are more sensitive sensors based on LSPR shift than their counterparts with a small AR (14, 15). Hence, the selection of Au cores is very important.

According to reaction equation, one  $\text{Cu}^{2+}$  etches one Ag atom. We can use the LSPR peak shift ( $\Delta\text{LSPR} = \text{LSPR}_{\text{Au}} - \text{LSPR}_{\text{Au@Ag}}$ ) per Ag amount to characterize the detection sensitivity. As mentioned above, the AR of the rod is the critical factor in determining LSPR position. We first investigated its effect on sensitivity using numerical simulation (finite element method, FEM). As the core of Au@Ag probe, the AR of the Au NR affects greatly the LSPR position of the probe and thus the probe sensitivity. For instance, for the Au core with an effective radius of 16.5 nm (volume =  $18973 \text{ nm}^3$ ), by changing its AR from 3.07 to 6.00 (table S1), we can improve sensitivity from 38 nm to 59 nm per unit volume Ag (Figure 1A). For simplicity, we define Ag shell volume of  $4460 \text{ nm}^3$  as the unit Ag (corresponding to 1 nm thick Ag on the Au core with the volume of  $18973 \text{ nm}^3$  and the AR of 4.51). The detailed effect of the core AR is given in Figure 1B and S1A&B. At the fixed core volume, the Au core with a higher AR gives better sensitivity, in agreement with previous reports (14, 15). Apart from AR, the core volume is also a factor to be reckoned with as the unit Ag shell may cause distinctive AR variation for different core sizes. For example, at same AR of 4.51, the Au core with volume of  $20000 \text{ nm}^3$  exhibits a sensitivity of 38 nm per unit Ag whereas 105 nm per unit Ag is obtained by reducing core size to  $6000 \text{ nm}^3$ . It can be explained by a larger AR change in the small core probe (from 4.51 to 3.54) than the large core probe (from 4.51 to 4.05) upon unit Ag deposition (S1D). At the fixed core AR, the probes with smaller cores are obviously more sensitive (Figure 1C and S1C). Therefore, probes with small volumes and large ARs of Au cores are ideal for sensitive detection. Once the Au cores are chosen, the probe sensitivity is determined as we tailor the shifted LSPR position of the control sample to that of the Au core, because this position is the most sensitive position to Ag change (Figure 1D: the slope of zero has the biggest value). Considering the corresponding relation between Ag and  $\text{Cu}^{2+}$ , the Ag amount is used to regulate the dynamic range: low Ag amount means a narrow dynamic range (Figure 1D). Effects of the three factors on the figure of merit (FOM, defined as  $\Delta\text{LSPR}/\text{fwhm}$ , where fwhm is the full width at half-maximum of the resonance) are shown in Figure S2 (5). Smaller Au NR gives higher FOM. For the AR of Au core, the maximum FOM is achieved with AR between 3 and 4. And thinner Ag shows larger FOM.

In order to confirm our simulations, we use three different Au NR cores and grow different amounts of Ag (12 samples) to demonstrate the LSPR sensitivity. Figure S3 shows the TEM images of the Au NR cores and Au@Ag NRs. The Au NR-795nm (LSPR maximum at 795 nm) with the largest AR of  $\sim 3.73$  (table S2) has the medium core volume. The Au NR-655 nm (AR:  $\sim 2.36$ ) has the largest core volume. Mini Au NR-655nm (AR:  $\sim 2.46$ ) shows the similar LSPR maximum to Au NR-655nm but has the smallest core volume among the three Au cores. As Figure 1E shows, the Au NR-795nm with a larger AR exhibits a larger LSPR shift than the mini Au NR-655nm after depositing same amount of Ag. And the mini Au NR-655 nm with a smaller core volume shows more LSPR shift than Au NR-655nm. The experiment results are well agreed with our

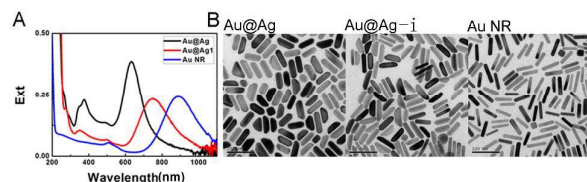


**Figure 2.** (A) Extinction spectra and (B) TEM images of Au NR core, the probe Au@Ag and one intermediate state (Au@Ag-i) of the etch process.

simulation results. Likewise, it is also verified by the measured ARs from TEM analysis that the change of sensitivity is due to the different AR variations per unit Ag for different samples (table S2). Corresponding extinction spectra are presented in Figure S4.

Furthermore, the calculated extinction spectra for asymmetric Ag shells are similar to those of conformal ones (Figure S5). So, for protein detection, we use the Au core (AR about 4.6) with LSPR maximum at ~ 890 nm (Figure 2) to grow asymmetric Ag shell as its growth method is very convenient. The core size is chosen to be ~ 10000 nm<sup>3</sup> by taking account of both probe sensitivity and rod stability. Figure 2 shows the extinction spectra and the TEM images of the nanoparticles we use. The LSPR maximum of the Au@Ag is about 630 nm and can give the maximum range of the LSPR peak shift of 250 nm. Au@Ag-i is one intermediate state of the etching process. Table S3 lists the measured dimension changes during etching.

Our protein detection is based on the etching of Ag shell by Cu<sup>2+</sup> with the assistance of BCA. Figure 3A is a typical extinction spectra evolution of Au@Ag etching by Cu<sup>2+</sup>/BCA pair. The LSPR peak continuously shifts to red during etching. And Cu<sup>+</sup>-BCA complex's characteristic absorption peak at 562 nm appears and increases in absorbance intensity with time. First, BCA/Cu<sup>2+</sup> ratio is optimized.

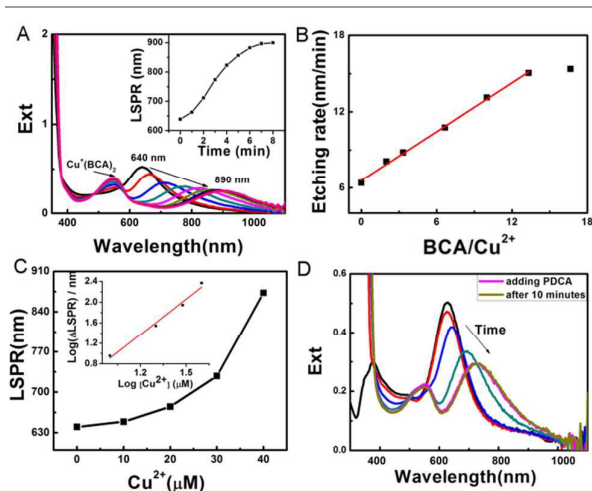


**Figure 3.** (A) Evolution of Au@Ag extinction spectra during etching by 50 μM Cu<sup>2+</sup> ions and 500 μM BCA, inset: LSPR wavelength vs. Time. (B) Etching rate vs. BCA/Cu<sup>2+</sup> ratio, [Cu<sup>2+</sup>] = 30 μM. (C) Effect of Cu<sup>2+</sup> concentration on the LSPR wavelength, BCA/Cu<sup>2+</sup> = 10. (D) Extinction spectra evolution of Au@Ag before and after adding 100 μM PDCA, [Cu<sup>2+</sup>] = 50 μM, [BCA] = 500 μM.

With the increase of BCA, the etching rate first increases and then reaches a plateau (15 nm/min, Figure 3B). In the absence of BCA, Cu<sup>2+</sup> alone assists the etching of Ag shell by dissolved oxygen with a slower rate (6 nm/min, Figure S6Aa). Cu<sup>+</sup>-BCA complex does not cause observable influence on the extinction spectra of Au@Ag (Figure S6B). With optimal BCA/Cu<sup>2+</sup> ratio of 10/1, we further investigated the effect of Cu<sup>2+</sup> amount as it is the quantification basis of our method. As Figure 3C shows, increasing Cu<sup>2+</sup>, more red-shift in LSPR wavelength is observed as we expected (corresponding extinction spectra shown in Figure S7). As each Cu<sup>2+</sup> oxidizes one Ag atom, we choose a slightly higher amount of cupric ions in comparison with Ag shell to fully utilize the LSPR shift range. Cupric ions blocking agent, 2, 6-pyridinedicarboxylic acid (PDCA), is used to stop etching at optimal reaction time. Figure 3D shows PDCA is efficient in stopping etching.

Other influence effects including cetyltrimethylammonium bromide (CTAB), Br<sup>-</sup>, protein adsorption, and pH values are also optimized. The surfactant CTAB plays the dual roles in etching reaction: stabilizing the Au@Ag suspension and providing Br<sup>-</sup> to bind the dissolved Ag<sup>+</sup>. The etching rate vs. CTAB concentration shows a non-monotonic change. When no extra CTAB is added in the etching solution, the etching rate was very slow due to lack of Br<sup>-</sup> and the Ag shell cannot be etched completely (Figure S8A and B). Adding small amount of CTAB, the etching rate rises steeply and reaches the maximum at 50 μM due to the complexing of Ag<sup>+</sup> by Br<sup>-</sup>. The role of Br<sup>-</sup> is visualized by adding KBr. The etching rate increases significantly with KBr concentration (Figure S8C). At CTAB concentration of 0.5 mM, the etching rate falls steeply. From 0.5 mM to 0.1 M, etching rate shows slight increase. Apart from the above two main roles, existence of CTAB also helps reduce the interference of protein adsorption on etching. By controlling CTAB amount in the etch solution, we greatly reduced the influence of protein adsorption. As Figure S9 shows, at 0.1 M CTAB, BSA amount poses a negligible effect on Cu<sup>2+</sup>/BCA pair-caused LSPR shift (no incubation of protein, Cu<sup>2+</sup>, and BCA). In contrast, with 5 mM CTAB, protein adsorption strongly hinders the etching of Ag shell and results in less LSPR shift. The reduced protein adsorption at high CTAB concentration is supported by Zeta potential change of Au@Ag due to the BSA adsorption. Compared with 0.5 mM CTAB, 0.1 M CTAB can effectively prevent the decrease of Zeta potential of Au@Ag (Table S4). So we use 0.1M CTAB as our optimal condition. The fastest etching rate was achieved at pH value of 6 (Figure S8D).

The standard curve with a series of gradient concentrations of BSA was obtained from the two step method. We call it SPR-BCA assay. The first step is a simplified BCA assay by the reduction of Cu<sup>2+</sup> to Cu<sup>+</sup> by protein. The BSA standards were obtained by stepwise dilution in a pH 7.4 buffer solution. The second step is the etching of Au@Ag. After the etching agent from step 1 was added to the Au@Ag solution for 7 minutes, PDCA was added to stop the reaction. The kinetic process was recorded. Figure S10A shows the LSPR variation with time. At the eighth minute, the LSPR wavelength of the control sample (without BSA) is ~ 890 nm close to the LSPR of Au core as we have designed. The extinction spectra of all the standard samples (repeated 3 times for each sample) at the 8th minute are shown in Figure S10B. Figure 4A shows the standard curve for the detection of BSA. The logarithm of (255-

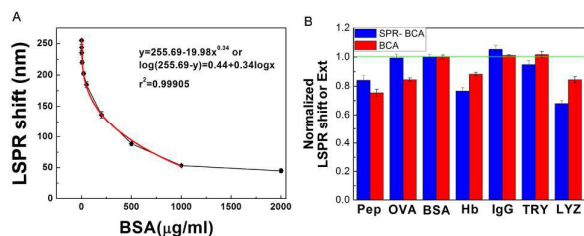


**Figure 4.** (A) Standard curve of SPR-BCA assay for the detection of BSA; (B) Response characteristics for different proteins, normalized LSPR shift of SPR-BCA assay and normalized absorbance (562 nm) of BCA assay for proteins relative to BSA.

LSPR shift) is well linear with the logarithm of BSA concentration from 0.5 to 1000  $\mu\text{g/ml}$ , with the regression equation  $\log(255 - y) = 0.44 + 0.34 \log x$  ( $R^2 = 0.9991$ ) and the limit of detection (LOD) is 3.4 ng/ml (3 S/N, signal-noise-ratio). In addition, at certain concentration range, protein amount can be also quantified using extinction intensity. As the inset in Figure S12A shows, the logarithm of the extinction intensity at 780 nm is well linear with the logarithm of BSA concentration between 0.5 and 200  $\mu\text{g/ml}$ . For BCA assay, the common method used to determine protein concentration in laboratories (16), we obtained a linear range from 50 - 1000  $\mu\text{g/ml}$  (Figure S12B). Enhanced BCA assay can determine total protein content down to 0.5  $\mu\text{g/ml}$  with a linear working range of 0.5 - 40  $\mu\text{g/ml}$ . Another protein quantification Biuret method, on the other hand, has the LOD in mg range (13). Other protein detection methods, such as the Lowry protein assay and Bradford protein assay, their micro detection range are in  $\mu\text{g}$  range (17). In comparison with commonly used protein quantification methods, SPR-BCA assay is obviously beneficial with a broader detection range and higher sensitivity. Recently, more protein quantification methods are found. Based on gold nanoparticles aggregation, Jiang's group shows a LOD (3 S/N, signal-noise-ratio) of 0.2  $\mu\text{g/ml}$  with a broad linear range of 30 - 2500  $\mu\text{g/ml}$  for BSA (18). Tang et al. reported a protein assay method based on an aggregation-induced emission fluorophore with a linear range of 0.5-100  $\mu\text{g/ml}$  (19). Our SPR-BCA assay is more sensitive and has a wider detection range.

To test the universality of our method, we examined the responses of different proteins. Table S5 shows the parameters of the proteins we selected. They involve a broad range of molecular weight, pI, as well as numbers of subunits and shapes. Figure 4B shows the response characteristics for different proteins to BSA of the two methods. For SPR-BCA and conventional BCA assay, the average value is 0.900 and 0.910, respectively and the standard deviation is 0.138 and 0.103, respectively. It indicates that SPR-BCA assay shows a universal applicability to various proteins.

## Conclusions

In summary, we present an SPR detection method to quantify proteins by building up the relationship between LSPR peak shift of Au@Ag nanorods and protein amount via  $\text{Cu}^{2+}$ /BCA pair bridged protein oxidation and Au@Ag etching. The SPR-BCA assay shows

obviously improved sensitivity and a wide dynamic range (0.5 to 1000  $\mu\text{g/ml}$ ) compared with conventional BCA assay. The universal applicability to various proteins further proves the potential of SPR-BCA assay in practical applications.

## Acknowledgements

The work was supported by the National Key Basic Research Program of China (2012CB934001) and the National Natural Science Foundation of China (Grant No. 21173056).

## Notes and references

- P. D. Howes, R. Chandrawati and M. M. Stevens, *Science*, 2014, 346, 1247390–12473910.
- M. Grzelczak and L. M. Liz-Marzán, *Langmuir*, 2013, 29, 4652–4663.
- S. N. Chen, Q. Zhao, F. Liu, H. W. Huang, L. Q. Wang, S. J. Yi, Y. L. Zeng and Y. Chen, *Anal. Chem.*, 2013, 85, 9142–9147.
- P. D. Howes, S. Rana and M. M. Stevens, *Chem. Soc. Rev.*, 2014, 43, 3835–3853.
- K. M. Mayer and J. H. Hafner, *Chem. Rev.*, 2011, 111, 3828–3857.
- M. B. Cortie and A. M. McDonagh, *Chem. Rev.*, 2011, 111, 3713–3735.
- L. Polavarapu, J. Pérez-Juste, Q. H. Xu and L. M. Liz-Marzán, *J. Mater. Chem. C*, 2014, 2, 7460–7476.
- R. de la Rica and M. M. Stevens, *Nat. Nanotechnol.*, 2012, 7, 821–824.
- L. Rodríguez-Lorenzo, R. de la Rica, R. A. Álvarez-Puebla, L. M. Liz-Marzán and M. M. Stevens, *Nat Mater*, 2012, 11, 604–7.
- C. J. DeSantis, R. G. Weiner, A. Radmilovic, M. M. Bower and S. E. Skrabalak, *J. Phys. Chem. Lett.*, 2013, 4, 3072–3082.
- J. Becker, I. Zins, A. Jakab, Y. Khalavka, O. Schubert and C. Sönnichsen, *Nano Lett.*, 2008, 8, 1719–1723.
- T. Wen, H. Zhang, X. P. Tang, W. G. Chu, W. Q. Liu, Y. L. Ji, Z. J. Hu, S. Hou, X. N. Hu and X. C. Wu, *J. Phys. Chem. C*, 2013, 117, 25769–25777.
- A. Gornall, C. J. Bardawill and M. David, *J. Biol. Chem.*, 1949, 177, 751–766.
- D. E. Charles, D. Aherne, M. Gara, D. M. Ledwith, Y. K. Gun'ko, J. M. Kelly, W. J. Blau and M. E. Brennan-Fournet, *ACS Nano.*, 2010, 4, 55–64.
- H. J. Chen, X. S. Kou, Z. Yang, W. H. Ni and J. F. Wang, *Langmuir*, 2008, 24, 5233–5237.
- P. K. Smith, R. I. Krohn, G. T. Hermanson, A. K. Mallia, F. H. Gartner, M. D. Provenzano, E. K. Fujimoto, N. M. Goeke, B. J. Olson and D. C. Klenk, *Anal Biochem.*, 1985, 150, 76–85.
- J. E. Noble, M. J. Bailey, *Methods Enzymol.* 2009, 463, 73–95.
- K. Zhu, Y. Zhang, S. He, W. W. Chen, J. Z. Shen, Z. Wang and X. Y. Jiang, *Anal. Chem.*, 2012, 84, 4267–4270.
- H. Tong, Y. Hong, Y. Dong, M. Häussler, Z. Li, J. W. Lam, Y. Dong, H. H. Sung, I. D. Williams, B. Z. Tang, *J. Phys. Chem. B* 2007, 111, 11817–11823.